Elastic properties of central-force networks with bond-length mismatch

M. F. Thorpe* and E. J. Garboczi
National Institute of Standards and Technology, Building Materials Division, B348/226, Gaithersburg, Maryland 20899
(Received 26 February 1990)

We study a triangular network containing two kinds of Hooke springs with different natural lengths. If the two spring constants are the same, we can solve the model exactly and show that Vegard's law is obeyed, irrespective of whether the bonds are arranged randomly or in a correlated way. A more complete description of these networks is obtained through the mean lengths, the length fluctuations, and the strain energy. The complete distribution of bond lengths is obtained numerically and shows an interesting and unexpected symmetry for the random case. Finally we show that numerical results for a similar system, but with different force constants as well as different natural lengths, can be well accounted for by using an effective-medium theory that reduces to the exact results when the two spring constants are made equal. These lattices can be described very accurately up to about 50% length mismatches, when "pleating" occurs and the lattices develop local instabilities.

I. INTRODUCTION

All solid elastic materials, in the absence of an induced external stress, can relax to a state of zero macroscopic stress. More precisely, this means that, when an external strain is applied to a material in this reference state, there is no term in the strain-energy density that is linear in the strain. This reference state defines a natural size or length scale for the material. One general way to define this length would be by the edge length of a cube formed from a unit mass of the solid at standard temperature and pressure, for example. In the case of an undistorted crystalline solid with known crystal structure, this prescription is equivalent to specifying the lattice, although see the caution at the end of Sec. V.

A state of zero macroscopic stress does not, however, necessarily imply a state of zero strain energy. Only if the same natural length applies throughout the solid is the internal strain energy also zero. This would be the case for a perfectly crystalline solid. In general, however, there can be "mismatches" in natural length between different regions in the interior of a solid. In the absence of an applied stress, this will lead to an effective macroscopic natural length that is some microscopically weighted average over the internal lengths.

There are many examples of this kind of behavior and we list a few gleaned from the recent literature to illustrate the broad range of materials in which natural length mismatch between "matrix" and "inclusions" is important. Boron- and/or germanium-doped silicon is a good example of natural length mismatch, as the dopant atoms try to fill silicon-sized holes in the silicon lattice. Boron, being smaller than silicon, induces lattice shrinkage while germanium, being larger than silicon, induces lattice expansion.[1,2] In boron-doped silicon, hydrogen passivation of the boron acceptors causes the effective natural length of the material to increase because of natural length increases at the boron sites due to the formation of B-H complexes.[3] Lower-density amorphous regions in radiation-damaged ceramics[4] and oxide precipitates in oxygen-implanted Si-on-SiO_2 structures[5] can produce natural length mismatch and stored strain energy. Natural length mismatch is also an important factor driving the amorphization of Mn-implanted Al films and single crystals[6] as well as the formability of a whole range of metallic glass alloys.[7]

In the area of materials science, natural length mismatch is exploited to strengthen glass using the process of chemical tempering.[8,9] In this process, larger ions are exchanged for smaller ions in the glass network, thereby inducing stored strain energy associated with compressive stress in the surface.[10] The surface compression tends to deactivate the surface cracks, which are the strength-limiting flaws,[8,11] thereby increasing the overall tensile strength by roughly the amount of the surface compressive stress.[12] In the area of engineering materials, the durability of concrete is controlled to a large extent by natural length mismatch. The aggregate that is mixed with portland cement and water to make concrete can react with alkaline element constituents. The products that are formed have a larger natural length than the original aggregate, inducing intense local compressive and tensile stresses, which can cause cracking.[13] Sulfate ions can attack cement paste, resulting in chemically induced local expansion and other deleterious effects.[13]

Finally, almost any kind of elastic solid that is formed at least partially by the consumption of a liquid constituent is subject to tensile stresses due to natural length mismatch arising from the collapse of capillary pores as the liquid is removed. The ubiquitous "mud-cracking" seen in dry lake beds is a good example of this behavior,[14] as is residual tensile stress and cracking in sol-gel films.[15]

In this paper, we focus on a simple central-force model that can describe the general features of this phenomenon. It is an extension of a previous model[16] and consists of a two-dimensional triangular network of Hooke's-law springs with natural lengths L_{ij} and force constants K_{ij}. Natural length mismatch is built in from

the start by allowing the lengths L_{ij} to be random variables. In this paper we concentrate our attention on the case where there are only two kinds of springs, A and B. The network is allowed to relax to its preferred size by minimizing the energy.

The layout of this paper is as follows. In Sec. II we define the notation, and give some general results that can be derived without any detailed calculation. In Sec. III we present the exact solution when the spring constants are all equal. In Sec. IV we show how correlations can be treated. These correlations introduce a local tendency to cluster. It is shown that the work of Sec. III can be generalized to cover this case. Details of the statistics associated with the correlations are given in Appendix A. In Sec. V we develop an effective-medium theory that is shown to be rather accurate when the spring constants are not all equal. The general problem of what is meant by "length" is also discussed, and it is shown that for triangular networks, the microscopic and macroscopic definitions do agree. In Sec. VI we give a general discussion and examine the length probability distributions. It is shown that the A and B distributions are identical (of course shifted and with different weights) when the spring constants are equal and the distribution of bond lengths is random. We also discuss the elastic moduli. We show that the harmonic approximation is excellent until "pleating" occurs. Throughout the paper our exact (or effective-medium results) are compared with computer simulations.

II. GENERAL RESULTS

We consider a stable lattice such as the triangular net shown in Fig. 1. Other two-dimensional lattices, such as the square net and the honeycomb lattice, are unstable under purely nearest-neighbor central forces.[17] In three dimensions, the face-centered-cubic lattice is stable under nearest-neighbor central forces, and the formalism in this paper would apply equally well for the face-centered-cubic lattice or any other stable lattice. We retain the conductivity of the lattice in Fig. 1, but the bonds have natural (unstretched) lengths L_{ij}^0 with spring constants K_{ij}. Much of our theory applies quite generally, but to be specific, we consider a distribution, which can be random or correlated, of *two kinds of bonds*. One of these has a natural length L_A^0, spring constant K_A, and occurs with probability $1-x$. The other has a natural length L_B^0, spring constant K_B, and occurs with probability x. This may be thought of as a solid $A_{1-x}B_x$, where A,B refer to *bonds* and not to sites. This solid is described by a potential

$$V=\tfrac{1}{2}\sum_{\langle ij\rangle} K_{ij}(|\mathbf{R}_i-\mathbf{R}_j|-L_{ij}^0)^2 . \tag{1}$$

Here L_{ij}^0 can take on the two values L_A^0 and L_B^0 with probability $1-x$ and x, respectively. The summation goes over all nearest-neighbor bonds ij and the angular brackets denote that nearest-neighbor sites are only counted once. The vector $\mathbf{R}_i$ goes to a site at the end of the bond ij from some (arbitrary) origin. The potential (1) can be minimized with respect to the $\mathbf{R}_i$ to give

$$0=\sum_i K_{ij}[(\mathbf{R}_i-\mathbf{R}_j)-L_{ij}^0\hat{\mathbf{R}}_{ij}] . \tag{2}$$

Notice that $\mathbf{R}_i$ is now the *relaxed* vector and so $\hat{\mathbf{R}}_{ij}$ is a unit vector along the *relaxed* bond direction. These equations determine the equilibrium positions of all the sites. An example is shown in Fig. 2, where L_B^0 is 30% larger than L_A^0, and $K_A=K_B$. Here the equilibrium of the sample was determined numerically, using standard techniques.[17]

The average bond length is defined by

$$\langle L\rangle=\frac{1}{N}\sum_{\langle ij\rangle} L_{ij} \tag{3}$$

with similar definitions for $\langle L_A\rangle$ and $\langle L_B\rangle$ for the A- and B-type bonds. Here N is the number of bonds in the lattice and we are always concerned with the thermodynamic limit $N\to\infty$. By definition

$$\langle L\rangle=(1-x)\langle L_A\rangle+x\langle L_B\rangle . \tag{4}$$

We have chosen the notation to parallel that of Thorpe, Wei, and Mahanti[18] who have recently studied similar

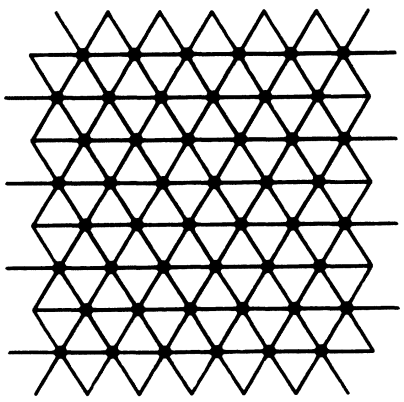

FIG. 1. A perfect undistorted triangular network.

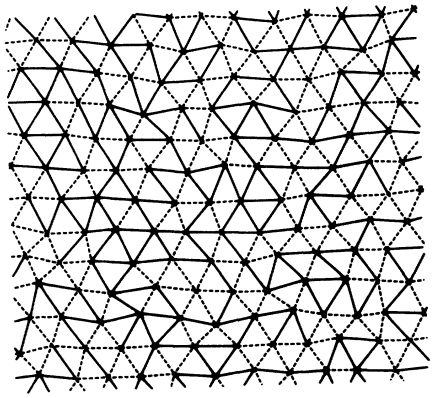

FIG. 2. A piece of a relaxed triangular network. The short bonds are shown as dashes and the long bonds by solid lines. The sample shown has equal numbers of short and long bonds and the natural length of the long bonds is 30% greater than the natural length of the short bonds. The two spring constants are equal.

problems associated with two-dimensional alloys in intercalated graphite and in clays. The present situation is formally quite similar, but more complex, because here the displacements are not uniaxial. Nevertheless, many of the results carry over.[18,19]

The Feynman-Hellman theorem[20] has been shown to be useful in this type of problem.[18] In the present context, this theorem states that

$$\frac{\partial}{\partial p}\langle \varepsilon \rangle = \left\langle \frac{\partial \varepsilon}{\partial p} \right\rangle , \tag{5}$$

where the energy $\varepsilon = V/N$ depends explicitly on some parameter p. From Eq. (1), we see that p can be set equal to L_A^0 or L_B^0, which leads to

$$\begin{aligned} K_A(1-x)(\langle L_A \rangle - L_A^0) &= -\frac{\partial \varepsilon}{\partial L_A^0} , \\ K_B x(\langle L_B \rangle - L_B^0) &= -\frac{\partial \varepsilon}{\partial L_B^0} . \end{aligned} \tag{6}$$

Equation (6) involve no assumptions about small displacements. However, they are not very useful as they stand. If we assume that the displacements from a perfect triangular network are small, and if we note that there is no net macroscopic force on the system in equilibrium, we find that

$$(1-x)K_A(\langle L_A \rangle - L_A^0) + xK_B(\langle L_B \rangle - L_B^0) = 0 , \tag{7}$$

which states that the net macroscopic tension is zero perpendicular (or parallel) to any line drawn parallel to the bonds in Fig. 2. This line is imagined to be a rigid mathematical line. This procedure is equivalent to replacing the $\hat{\mathbf{R}}_{ij}$ in Eq. (2) by the undistorted unit bond vectors from Fig. 1. Combining Eqs. (6) and (7), we see that

$$\frac{\partial \varepsilon}{\partial L_A^0} + \frac{\partial \varepsilon}{\partial L_B^0} = 0 \tag{8}$$

and hence the energy can only depend on the difference $(L_B^0 - L_A^0)$. However, we can invoke dimensional arguments from the potential (1) to see that the energy must be proportional to $(L_B^0 - L_A^0)^2$ and therefore may be written as

$$\varepsilon = \tfrac{1}{2}(K_A K_B)^{1/2} x(1-x)(L_B^0 - L_A^0)^2 F_\varepsilon(x, K_B/K_A) . \tag{9}$$

It is convenient to include a factor $x(1-x)$ in (9) when defining the dimensionless function $F_\varepsilon(x, K_B/K_A)$. A similar result was found previously.[18,19] Here (9) is only true in the small displacement limit. The symmetry of the potential (1) under the interchange $A \leftrightarrow B$ together wit $x \leftrightarrow 1-x$ puts a restriction on the function, namely $F_\varepsilon(x, K_B/K_A) = F_\varepsilon(1-x, K_A/K_B)$. Note that if any one of the quantities $\langle L \rangle$, $\langle L_A \rangle$, and $\langle L_B \rangle$ are known, then the other two can be found using Eqs. (4) and (7), unless $K_A = K_B$. Using (6), (7), and (9), we find that

$$\begin{aligned} \langle L \rangle &= (1-x)L_A^0 + xL_B^0 + \frac{2\varepsilon(K_B - K_A)}{K_A K_B (L_B^0 - L_A^0)} , \\ \langle L_A \rangle &= L_A^0 + \frac{2\varepsilon}{(1-x)K_A(L_B^0 - L_A^0)} , \\ \langle L_B \rangle &= L_B^0 - \frac{2\varepsilon}{xK_B(L_B^0 - L_A^0)} . \end{aligned} \tag{10}$$

These are important general results which show that if $K_B > K_A$, the mean length lies above Vegard's law[21] (superlinear) and if $K_B < K_A$, the mean length lies below Vegard's law (sublinear). This result is independent of any correlations in bond positions that may exist. In the extreme case of complete phase separation, $\varepsilon = 0$ and Vegard's law[21] is recovered from (10) as expected. The interface energy is negligibly small in the thermodynamic limit. Note that we define $L_B^0 > L_A^0$ throughout this paper.

The Feynman-Hellman theorem (5) is also helpful in finding the fluctuations. If we set p equal to K_A and K_B, respectively, in (5), we find that

$$\begin{aligned} (1-x)\langle (L_A - L_A^0)^2 \rangle &= 2\frac{\partial \varepsilon}{\partial K_A} , \\ x\langle (L_B - L_B^0)^2 \rangle &= 2\frac{\partial \varepsilon}{\partial K_B} . \end{aligned} \tag{11}$$

The total fluctuations are given by[18]

$$\begin{aligned} \langle (L - \langle L \rangle)^2 \rangle = (1-x)\langle (L_A - \langle L_A \rangle)^2 \rangle \\ + x\langle (L_B - \langle L_B \rangle)^2 \rangle \\ + x(1-x)(\langle L_A \rangle - \langle L_B \rangle)^2 , \end{aligned} \tag{12}$$

which follows directly from the definitions. Using (9) and (11), the fluctuations (12) become

$$\begin{aligned} \langle (L - \langle L \rangle)^2 \rangle = 2\frac{\partial \varepsilon}{\partial K_A} + 2\frac{\partial \varepsilon}{\partial K_B} + x(1-x)(L_B^0 - L_A^0)^2 \\ - 4\varepsilon^2 \left[\frac{1}{K_B} - \frac{1}{K_A} \right]^2 \Big/ (L_B^0 - L_A^0)^2 \\ - 4\varepsilon[(1-x)K_A + xK_B]/(K_A K_B) . \end{aligned} \tag{13}$$

The general relations (9)–(13) are particularly useful when $K_A = K_B$. We obtain Vegard's law[21] directly from (10)

$$\langle L \rangle = (1-x)L_A^0 + xL_B^0 . \tag{14}$$

No assumptions have been made in this derivation, so that Vegard's law (14) is proved to be true for any *arrangement of bonds.* Two extreme cases are a completely random arrangement and phase separation. An intermediate case, with correlations, is studied in Sec. IV. The fluctuations in (13) become

$$\langle (L - \langle L \rangle)^2 \rangle = 2\frac{\partial \varepsilon}{\partial K} + x(1-x)(L_B^0 - L_A^0)^2 - 4\varepsilon/K . \tag{15}$$

Using (12) we may also show that

$$(1-x)\langle(L_A-\langle L_A\rangle)^2\rangle+x\langle(L_B-\langle L_B\rangle)^2\rangle$$
$$=2\frac{\partial\varepsilon}{\partial K}-4\varepsilon^2/[K^2x(1-x)(L_B^0-L_A^0)^2]\ . \quad (16)$$

It is convenient to define a local *dimensionless length* d_{ij} such that

$$L_{ij}=L_A^0+d_{ij}(L_B^0-L_A^0)\ , \quad (17)$$

where $d_{ij}=0$ or 1 given by L_A^0 or L_B^0, respectively. Then the general results of this section can be summarized as follows:

$$\langle d\rangle=x\ ,$$
$$\langle d_A\rangle=x[1-a^*(x)]\ , \quad (18)$$
$$\langle d_B\rangle=1-(1-x)[1-a^*(x)]\ .$$

Note that the difference $\langle d_B\rangle-\langle d_A\rangle=a^*(x)$ gives a direct measure of $a^*(x)$. The quantity $a^*(x)=1-F_\varepsilon(x,1)$ is used to link up with previously used notation,[17] and is also equivalent to the Watson integral W, used in other recent work.[18,19] The energy and the total fluctuations are given by

$$\varepsilon=\tfrac{1}{2}Kx(1-x)[1-a^*(x)]\ , \quad (19)$$
$$\langle(d-\langle d\rangle)^2\rangle=x(1-x)a^*(x)\ . \quad (20)$$

The relations (18)–(20) assume only that the displacements are small and $K_A=K_B$. The bonds can be randomly mixed or correlated. The degree of correlation determines the dependence of $a^*(x)$ on the concentration x. The individual fluctuations $\langle(d_A-\langle d_A\rangle)^2\rangle$ and $\langle(d_B-\langle d_B\rangle)^2\rangle$ cannot be found by the general arguments given in this section and have to be found from the more detailed considerations in Sec. III.

III. EXACT SOLUTION WHEN SPRING CONSTANTS ARE EQUAL

When the spring constants K_A and K_B associated with the A- and B-type bonds are equal, the model can be solved exactly in the small displacement limit. This solution closely parallels previous work.[18] The essential observation that makes the solution possible is that there is no randomness in the dynamical matrix. This exact solution plays a similar role here to the exact solution of the two-dimensional Ising model in statistical mechanics,[22] and can act as a guide in more complex situations.

Because of the general results of Sec. II, our main task is to calculate $a^*(x)$. We shall do this here for a random distribution of bonds. We imagine a reference lattice that is a perfect undistorted triangular network, as in Fig. 1, with all the bonds having the as yet undetermined mean length $\langle L\rangle$. Assuming small displacements $\mathbf{u}_i$ associated with the sites $\mathbf{R}_i$, we may write

$$\mathbf{L}_{ij}=\mathbf{R}_i-\mathbf{R}_j=\mathbf{L}+[(\mathbf{u}_i-\mathbf{u}_j)\cdot\hat{\mathbf{R}}_{ij}]\hat{\mathbf{R}}_{ij}\ , \quad (21)$$

where the $\hat{\mathbf{R}}_{ij}$ are unit vectors along the *undistorted* bond directions. Inserting this into (2), we find that

$$0=\sum_i K_{ij}[(\mathbf{u}_i-\mathbf{u}_j)\cdot\hat{\mathbf{R}}_{ij}-(\langle L\rangle-L_{ij}^0)]\hat{\mathbf{R}}_{ij}\ . \quad (22)$$

If all the $K_{ij}=K$, Eq. (22) can be rewritten in terms of the usual dynamical matrix $\underline{D}$ for the triangular net[23]

$$\underline{D}\mathbf{u}=\mathbf{v}\ , \quad (23)$$

where the column vector $\mathbf{v}$ is given by

$$\mathbf{v}_i=K\sum_j(L_{ij}^0-\langle L\rangle)\cdot\hat{\mathbf{R}}_{ij}\ . \quad (24)$$

Solving for the displacements $\mathbf{u}_i$ gives

$$\mathbf{u}=-\underline{G}\mathbf{v} \quad (25)$$

or in components

$$u_i^\alpha=-\sum_{j\beta}G_{ij}^{\alpha\beta}v_j^\beta\ , \quad (26)$$

where $\underline{G}$ is the usual Green function for the perfect system.[17,23] Combining (21), (24), and (25)

$$L_{ij}=\langle L\rangle+K\sum_{lm}[\hat{\mathbf{R}}_{ij}\cdot(\underline{G}_{im}-\underline{G}_{jm})\cdot\hat{\mathbf{R}}_{lm}](L_{lm}^0-\langle L\rangle)$$
$$=\langle L\rangle+2K\sum_{lm}(\hat{\mathbf{R}}_{ij}\cdot\underline{G}_{im}\cdot\hat{\mathbf{R}}_{lm})L_{lm}^0\ . \quad (27)$$

Equation (27) gives the actual length of the bond ij in terms of *all* the natural lengths L_{lm}^0. If we average over both sides of (27) we get an identity because for all sites i

$$\sum_j\hat{\mathbf{R}}_{ij}=0\ . \quad (28)$$

In order to facilitate the averaging, we introduce bond variables σ_{ij}, where $\sigma_{ij}=1$ if the bond ij is A, and $\sigma_{ij}=-1$ if ij is B. The concentration x is given by

$$\langle\sigma_{ij}\rangle=1-2x\ . \quad (29)$$

The average length of the A-type bonds $\langle L_A\rangle$ may be written

$$\langle L_A\rangle=\langle L\rangle+\frac{K}{4N(1-x)}\times\sum_{ijlm}\langle(1+\sigma_{ij})(1+\sigma_{lm})\rangle\times(\hat{\mathbf{R}}_{ij}\cdot\underline{G}_{im}\cdot\hat{\mathbf{R}}_{lm})(L_A^0-L_B^0)\ . \quad (30)$$

Comparing with the expression for $\langle d_A\rangle$ in (18) and remembering that the dimensionless lengths are introduced via (17), we can extract $a^*(x)$

$$a^*(x)=\frac{K}{4Nx(1-x)}\sum_{ijlm}\langle\sigma_{ij}\sigma_{lm}\rangle(\hat{\mathbf{R}}_{ij}\cdot\underline{G}_{im}\cdot\hat{\mathbf{R}}_{lm})\ . \quad (31)$$

The result (31) is completely general and allows the quantities needed in Eqs. (18)–(20) to be obtained. For a random distribution of bonds in the solid $A_{1-x}B_x$, the pair-correlation function is given by

$$\langle\sigma_{ij}\sigma_{lm}\rangle-\langle\sigma_{ij}\rangle\langle\sigma_{lm}\rangle=4x(1-x)\delta_{ij,lm}\ . \quad (32)$$

Only the nearest-neighbor terms survive when we insert (32) into (31) to obtain

$$a^*(x)=a^*=2K[\hat{\mathbf{R}}_{ij}\cdot(\underline{G}_{ij}-\underline{G}_{ii})\cdot\hat{\mathbf{R}}_{ij}]$$
$$=2d/z$$
$$=\tfrac{2}{3}\ , \tag{33}$$

where ij is any nearest-neighbor bond. The result (33) is also given in Ref. 17 in a different context. For the triangular net, the dimension $d=2$ and the number of nearest neighbors $z=6$. The other important quantities of interest are the fluctuations $\langle(d_A-\langle d_A\rangle)^2\rangle$ and $\langle(d_B-\langle d_B\rangle)^2\rangle$. For the random distribution of bonds, a direct calculation can be made by squaring (27) and doing the appropriate projected averages. The surprising result is that the two fluctuations are *equal;* $\langle(d_A-\langle d_A\rangle)^2\rangle=\langle(d_B-\langle d_B\rangle)^2\rangle$. Therefore from (16) and (19), using the dimensionless units we find that

$$\langle(d_A-\langle d_A\rangle)^2\rangle=\langle(d_B-\langle d_B\rangle)^2\rangle$$
$$=x(1-x)a^*(1-a^*)\ . \tag{34}$$

The result (34) for the fluctuations can also be obtained as a special case of the more general results for the fluctuations when correlations are present, given in Sec. IV. The results for the random model are shown in Fig. 3 as a function of the composition x. The computer simulations were performed using the standard relaxation method,[17] and details of the parameters used are given in Appendix B. The natural lengths were taken to be $L_A^0=1.00$ and $L_B^0=1.01$. These lengths are not important as they scale out as long as the difference $(L_B^0-L_A^0)$ is sufficiently small. The agreement between the simulation and theory checks the accuracy of the simulation. The quantities $\langle d_A\rangle$ and $\langle d_B\rangle$ are straight lines because $a^*(x)$ is a constant. The energy and the fluctuations are parabolic in this case. We will show in Sec. VI that the nth moments of the A and B bond-length distributions are the same for all $n\geq 2$. This leads to *identical* line shapes for the A and B distributions. These distributions are centered on $\langle d_A\rangle$ and $\langle d_B\rangle$, and have weights $1-x$ and x, respectively.

IV. CORRELATED MODEL

We use a model described in Appendix A to introduce correlations between bonds. The model leads to correlations between nearest-neighbor bonds at a concentration x as given in Eqs. (A5) and (A6). The correlation between other pairs of bonds is zero. This simple short-ranged correlation allows us to calculate $a^*(x)$ explicitly from (31). The result is

$$a^*(x)=a^*-16[p(1-p)]^3(a^*/2+\tfrac{1}{2}-p_I^K)/[x(1-x)]\ , \tag{35}$$

where $a^*=2d/z=\frac{2}{3}$ for the triangular net as given in (33). The quantity p_I^K comes from a lattice integral over the nearest-neighbor shell and $16[p(1-p)]^3$ is just the nearest-neighbor correlation (A6) where p is determined by the concentration x. The lattice integral p_I^K also occurs when studying the bulk modulus in a sample with isolated sites removed;[24] for the triangular net $p_I^K=0.696$ and for the face-centered-cubic lattice $p_I^K=0.620$. Thus the correlations introduce an x dependence into $a^*(x)$. For the triangular net $a^*(0)=a^*(1)=\frac{2}{3}$ as in the random case, while $a^*(\frac{1}{2})=0.529$. For small x *or* $1-x$, we have

$$a^*(x)=\tfrac{2}{3}-0.106\sqrt{x(1-x)}\ . \tag{36}$$

This input can be used to calculate the quantities of interest in Eqs. (18)–(20) and the results are shown in Fig. 4. Notice that Vegard's law still holds for $\langle d\rangle$, but that $\langle d_A\rangle$ and $\langle d_B\rangle$ are no longer straight lines. The curvature is caused by the correlations and by the associated x dependence of $a^*(x)$. The energy and total fluctuations are no longer parabolic, although they are still symmetric about $x=\frac{1}{2}$.

The fluctuations in the A and B bond lengths can be obtained as follows. The rate of change of the energy

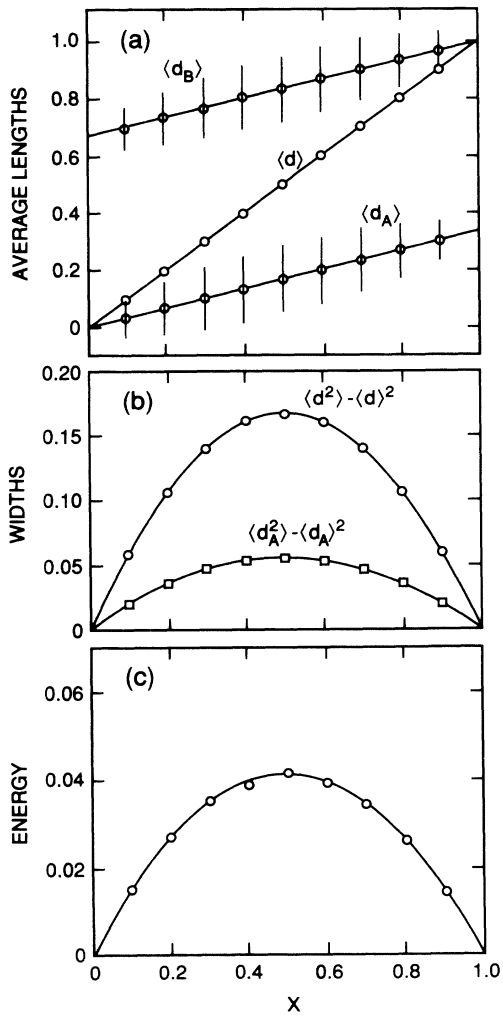

FIG. 3. Showing (a) average lengths $\langle d\rangle$, $\langle d_A\rangle$, and $\langle d_B\rangle$, (b) fluctuations in length, and (c) the energy per bond in units of $K(L_B^0-L_A^0)^2$ for the *random* triangular network with $K_A=K_B$. The solid lines are exact results and the symbols represent simulation results. The length of the vertical lines in (a) represents the width of the A and B peaks, calculated as the root-mean-square value as in (b) and obtained from the simulations.

with composition x is set equal to the total change in energy of the system when an A bond is replaced by a B bond. We obtain

$$\partial\varepsilon/\partial x = \frac{K}{2[1-a^*(x)]}[\langle(d_B-1)^2\rangle-\langle d_A^2\rangle] , \quad (37)$$

where ε is given by (19). The right-hand side of (37) is obtained by removing an A bond at random and replacing it by a B bond to give a configuration at a slightly larger x. The factor $[1-a^*(x)]$ arises from the effect of the lattice around the bond that is being changed. Thus we are led to the *difference* of the A and B fluctuations if we make a simple change inside the brackets in (37) to replace the natural lengths by the average lengths by adding and subtracting an appropriate term. The sum of the fluctuations can be obtained from the energy (19) directly.

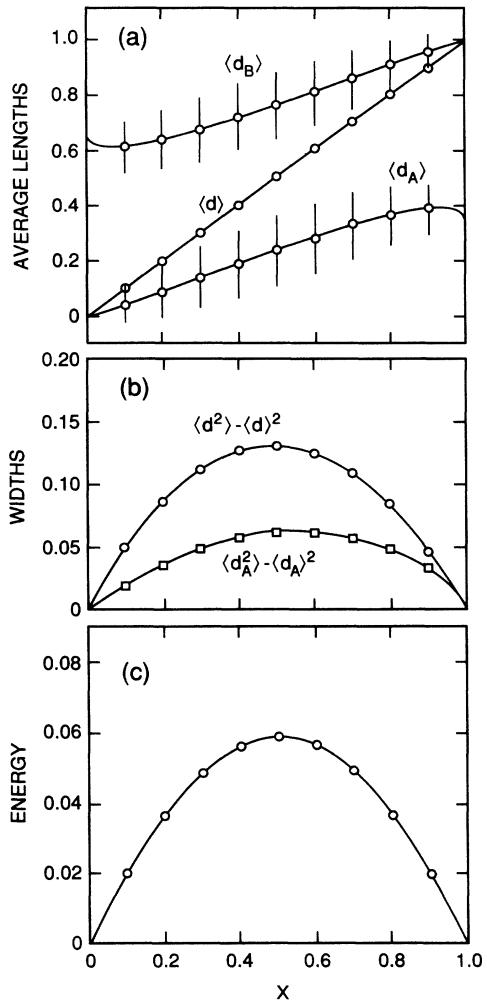

FIG. 4. Showing (a) average lengths $\langle d\rangle$, $\langle d_A\rangle$, and $\langle d_B\rangle$, (b) fluctuations in length, and (c) the energy in units of $K(L_B^0-L_A^0)^2$ for the *correlated* triangular network with $K_A=K_B$. The solid lines are exact results and the symbols represent simulation results. The length of the vertical lines in (a) represents the width of the A and B peaks, calculated as the root-mean-square value as in (b) and obtained from the simulations.

Thus we can extract the A and B bond-length fluctuations explicitly to give

$$\langle d_A^2\rangle-\langle d_A\rangle^2 = x(1-x)[1-a^*(x)]\frac{\partial[xa^*(x)]}{\partial x} , \quad (38)$$

$$\langle d_B^2\rangle-\langle d_B\rangle^2 = -x(1-x)[1-a^*(x)]\frac{\partial[(1-x)a^*(x)]}{\partial x} .$$

These results are also compared with the simulations in Fig. 4. When correlations are absent, the parameter $a^*(x)$ is independent of x and we recover the exact result (34). The arguments leading to (38) are not exact when correlations are present because the random replacement of A bonds by B bonds does not give a proper configuration at a concentration $x+dx$. This error appears to be very small, judged by the agreement between the simulations and the result (38). A similar line of reasoning has been used recently in a correlated multilayer model for binary alloys in graphite.[19]

V. EFFECTIVE-MEDIUM THEORY

We develop an effective-medium theory to handle the case $K_A\neq K_B$, which cannot be solved exactly. The work in this section follows the general ideas of Feng, Thorpe, and Garboczi,[17] who studied networks with different spring constants K_{ij} but no length mismatch. Recent work on alloys in layered systems extended this work to the case where there is length mismatch.[18,19] The result is expressed in terms of an effective spring constant K_e, where

$$K_e = K/a^* \quad (39)$$

and a^* is equivalent to the Watson integral[18,19] used previously. The self-consistency condition for the case of interest here with two kinds of bonds A,B can be written as

$$x(K-K_B)/(K_e'+K_B)+(1-x)(K-K_A)/(K_e'+K_A)=0 . \quad (40)$$

We note that this equation is the standard effective-medium equation for spring constants and *contains no lengths.* This is a direct consequence of the superposition principle for small displacements. The dynamics are unaffected by the (small) static distortions. Not only will the elastic constants be unaffected by the static distortions, but the complete phonon density of states will similarly be unaffected.

The problem is now effectively reduced to just two springs.[18] One of these springs is K_α, where α can be either A or B with probability $1-x$ or x, respectively. The other spring is $K_e'=K_e-K$, formed by removing the spring K which is in parallel. The total energy per site ε for a single impurity is given by

$$\varepsilon=\tfrac{1}{2}K_e'(L-L_e)^2+\tfrac{1}{2}K_\alpha(L-L_\alpha^0)^2 , \quad (41)$$

where L_e is the effective length which, like the effective spring constant K_e, is to be determined self-consistently. We are considering only a single impurity spring K_α in

Eq. (41). We minimize the energy ε with respect to L and obtain the local length L

$$L=(K_e'L_e+K_\alpha L_\alpha^0)/(K_e'+K_\alpha)\ . \tag{42}$$

Substituting this back in Eq. (41) gives the energy for a single impurity

$$\varepsilon=\tfrac{1}{2}(L_e-L_\alpha^0)^2K_e'K_\alpha/(K_e'+K_\alpha)\ . \tag{43}$$

Because the springs have different lengths, the postfactor in Eq. (43) comes from adding the two springs in series. A general energy expression can be written down by summing over all the different types of impurities which, in the spirit of the effective-medium theory, are assumed to be noninteracting. This energy expression is minimized with respect to L_e and expressions derived for the lengths and the energy. The details are the same as in Ref. 18 [see Eqs. (36) and (39)] and will not be repeated here.

The dimensionless length $\langle d\rangle$ is given by

$$\langle d\rangle=(\langle L\rangle-L_A^0)/(L_B^0-L_A^0)$$
$$=\frac{xK_B/(K_e'+K_B)}{xK_B/(K_e'+K_B)+(1-x)K_A/(K_e'+K_A)}\ , \tag{44}$$

which after some manipulation can be put into the form

$$\langle d\rangle=x+x(1-x)F_d\ , \tag{45}$$

where

$$F_d=\frac{K_eK_e'(K_B-K_A)}{K(K_e'+K_A)(K_e'+K_B)}\ .$$

Either directly, or using Eqs. (7) and (10), we can find $\langle d_A\rangle$ and $\langle d_B\rangle$,

$$\langle d_A\rangle=xK_eK_e'K_B/[K(K_e'+K_A)(K_e'+K_B)]\ ,$$
$$\langle d_B\rangle=1-(1-x)K_eK_e'K_A/[K(K_e'+K_A)(K_e'+K_B)]\ . \tag{46}$$

The energy is given by

$$\varepsilon=\tfrac{1}{2}(K_AK_B)^{1/2}x(1-x)(L_B^0-L_A^0)^2F_\varepsilon\ , \tag{47}$$

where

$$F_\varepsilon=K_eK_e'(K_AK_B)^{1/2}/[K(K_e'+K_A)(K_e'+K_B)]\ . \tag{48}$$

We note that

$$F_d/F_\varepsilon=(K_B-K_A)/(K_AK_B)^{1/2} \tag{49}$$

gives a useful relation as it is independent of any of the effective-medium parameters and exact,[18] as can be shown by the Feynman-Hellman theorem (5). Note that Eqs. (44)–(47) are consistent with the exact general results (10).

The fluctuations cannot be easily calculated within effective-medium theory. However, they can be obtained through the back door, using the Feynman-Hellman theorem Eq. (5), with p set equal to K_A and K_B, respectively. Using the effective medium Eq. (40) and differentiating (47) with respect to K_A, we find after some considerable algebra from (11)

$$\langle(d_A-\langle d_A\rangle)^2\rangle=\frac{x(1-x)\{(K_AK_BK_e^2)/[K(K_e'+K_A)^2(K_e'+K_B)]\}^2}{a^*/(1-a^*)+[(K-K_A)(K-K_B)]/[(K_e'+K_A)(K_e'+K_B)]}\ , \tag{50}$$

and a similar expression for $\langle(d_B-\langle d_B\rangle)^2\rangle$ with A and B interchanged in Eq. (50). Using Eq. (50), the fluctuations in d can be found using Eq. (12),

$$\langle(d-\langle d\rangle)^2\rangle=\frac{x(1-x)\{(K_AK_BK_e)/[K(K_e'+K_A)(K_e'+K_B)]\}^2/(1-a^*)}{a^*/(1-a^*)+[(K-K_A)(K-K_B)]/[(K_e'+K_A)(K_e'+K_B)]}\ . \tag{51}$$

We note that in the limit $K_A=K_B=K$, the exact results (18)–(20) are recovered.

In Figs. 5 and 6 we compare the effective-medium results, shown by dashed lines, with the computer simulations for $K_A=2K_B$ and $K_B=2K_A$. The overall agreement is excellent, although not rigorously exact. Notice that the average length $\langle L\rangle$ is sublinear in Fig. 5 and superlinear in Fig. 6 as required by the exact result (10).

Some of the formalism in the present section can also be applied to the correlated case if a^* is relaced everywhere by $a^*(x)$. The interpretation of Eq. (39) must be modified. Instead of applying a force F to the ends of a single bond, it is necessary to apply this force to *every* A-type bond. To avoid a net pressure on the body, forces $-Fx/(1-x)$ must also be applied to the ends of all the B-type bonds. That is, identical forces are applied to the complete set of the A bonds and another set to the B bonds. A generalized force constant $K/a^*(x)$ is obtained by this procedure, where the conjugate generalized displacement is the *mean* extension of the A-type bonds. If the bonds are uncorrelated, the effects of the other bonds of the same type being stretched cancels out, leading to Eq. (39). If the bonds are correlated, this is no longer the case and a^* must be replaced by $a^*(x)$. Note that when a single bond is stretched with forces F at either end, the effective spring constant is the same as in a perfect triangular net, as the order of the static distortion, and this extra distortion can be interchanged because the system is linear. These are subtle points that require some thought. Figures 7 and 8 show similar results to Figs. 5 and 6, but with the correlations between bonds included. Again the agreement between the effective-medium theory and the simulations in Figs. 7 and 8 is very good. We have not been able to develop a satisfactory expres-

sion for the A and B fluctuations when *both* correlations and different spring constants are present. Notice that $\langle d \rangle$ is weakly sensitive to the correlations here, unlike when $K_A = K_B$. Also the lengths $\langle d_A \rangle$ and $\langle d_B \rangle$ are no longer linear in the composition x. We also note that the computed value of F_d/F_ε, for all the cases where $K_A \neq K_B$, agrees with the exact result in (49) to within 0.04% or better, thus giving another check on the accuracy of the simulations.

In summary, we can state the following qualitative conclusions.

(a) Vegard's law for the average length $\langle d \rangle$ is obtained if and only if $K_A = K_B$. Sublinear or superlinear behavior is obtained if $K_A > K_B$ or $K_A < K_B$, respectively.

(b) The average lengths $\langle d_A \rangle$ and $\langle d_B \rangle$ are linear in the composition x, if and only if $K_A = K_B$ and there are no correlations.

(c) The strain energy ε is an even function of the composition if and only if $K_A = K_B$. The definition of length that we have used in this paper is the average bond length, which occurs naturally using our theoretical framework. It is also the quantity that is measured in extended x-ray-absorption fine-structure (EXAFS) experiments.[25] However, other definitions of length are possible which may or may not be equivalent. Each case must be examined carefully. Another natural definition of length would be a macroscopic length, which can be obtained from the square root of the total area. In the present example, this is the sum of the areas of all the local triangles of three bonds. If we consider a single equilateral triangle, with sides of length L and area $A = \sqrt{3}L^2/4$, then if the lengths of the three sides are

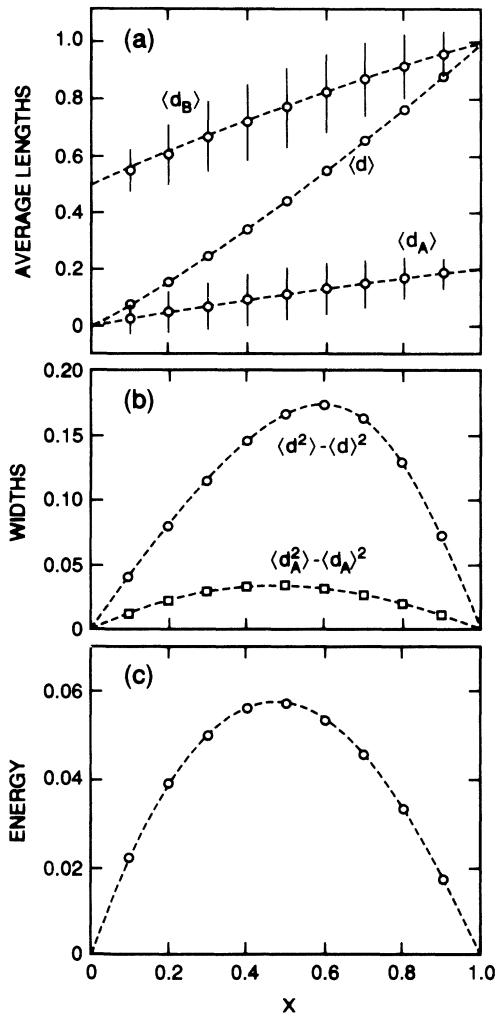

FIG. 5. Showing (a) average lengths $\langle d \rangle$, $\langle d_A \rangle$, and $\langle d_B \rangle$, (b) fluctuations in length, and (c) the energy in units of $K_B(L_B^0 - L_A^0)^2$ for a *random* triangular net with $K_A = 2K_B$. The dashed lines show results from effective-medium theory and the symbols represent simulation results. The length of the vertical lines in (a) represents the width of the A and B peaks, calculated as the root-mean-square value as in (b) and obtained from the simulations.

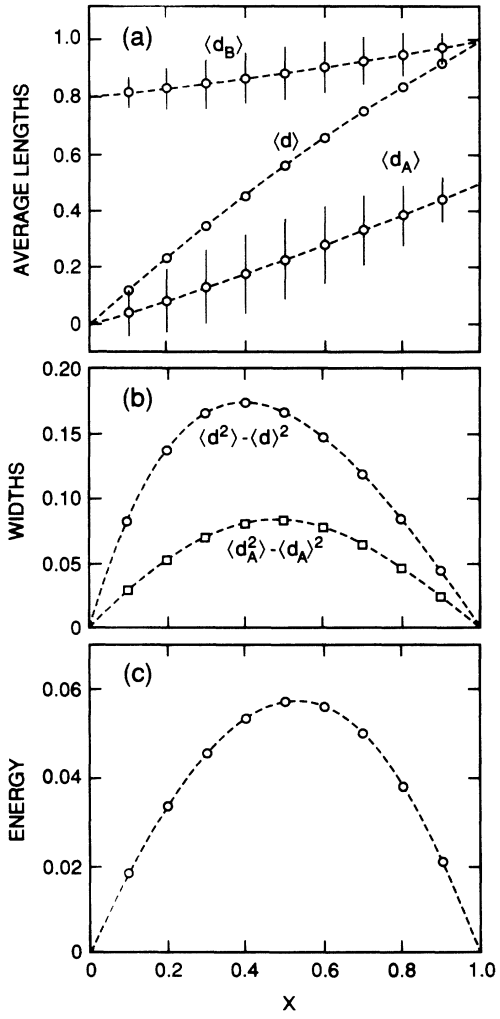

FIG. 6. Showing (a) average lengths $\langle d \rangle$, $\langle d_A \rangle$, and $\langle d_B \rangle$, (b) fluctuations in length, and (c) the energy in units of $K_A(L_B^0 - L_A^0)^2$ for a *random* triangular net with $K_B = 2K_A$. The dashed lines show results from effective-medium theory and the symbols represent simulation results. The length of the vertical lines in (a) represents the width of the A and B peaks, calculated as the root-mean-square value as in (b) and obtained from the simulations.

changed by ΔL_1, ΔL_2, and ΔL_3, the change in the area ΔA of the triangle is given to first order by

$$\Delta A = (L/\sqrt{12})(\Delta L_1 + \Delta L_2 + \Delta L_3) . \quad (52)$$

Summing over all triangles, we see that the condition $\langle \Delta L \rangle = 0$, which defines the mean undistorted triangular lattice discussed in Sec. III, is equivalent to $\langle \Delta A \rangle = 0$. Thus all macroscopic length averages will be equivalent to the mean bond length, and the two definitions of length are the same. The above argument only applies if the pure system is made up of equilateral triangles in two dimensions. It does *not* apply to triangles that are not equilateral, or to polygons with more than three sides. For example, the area of a square can be changed while keeping the lengths of all the sides fixed, so that an equation like (52) would not apply. When compared with our simulations, we find that the two definitions of length do indeed become equivalent as the length mismatch $(L_B^0 - L_A^0)/L_A^0$ tends to zero. The implications of these arguments for three-dimensional structures requires further thought. We note that a similar conclusion was reached in bilayer and multilayer compounds,[18,19] where the fact that all the displacements were uniaxial led to a similar equivalence between the average bond length and the macroscopic sample size.

VI. DISCUSSION

The nature of the disorder effect in the structure of random alloys can be more completely understood from the partial probability distribution functions of the lengths for the A- and B-type bonds. The length probability distributions $P(d)$, $P(d_B)$, and $P(d_A)$ are defined by

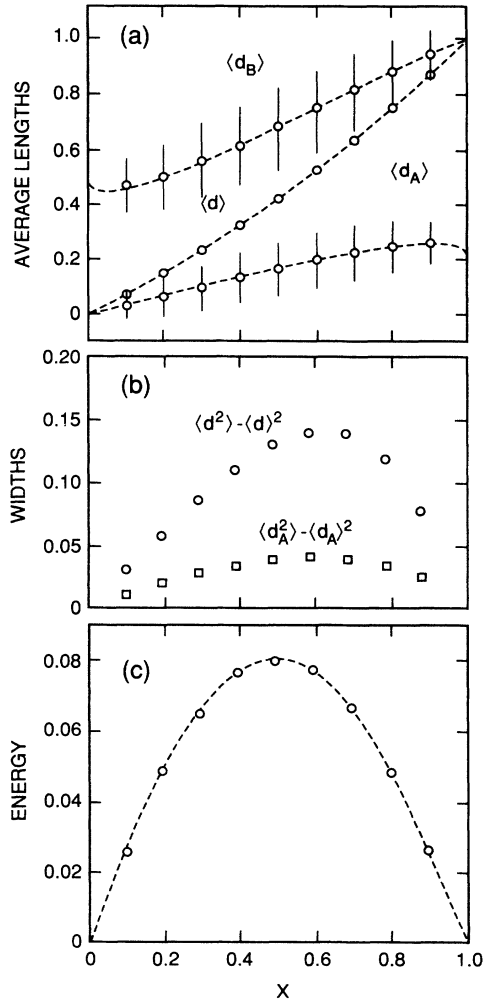

FIG. 7. Showing (a) average lengths $\langle d \rangle$, $\langle d_A \rangle$, and $\langle d_B \rangle$, (b) fluctuations in length, and (c) the energy in units of $K_B(L_B^0 - L_A^0)^2$ for a *correlated* triangular net with $K_A = 2K_B$. The dashed lines show results from effective-medium theory and the symbols represent simulation results. The length of the vertical lines in (a) represents the width of the A and B peaks, calculated as the root-mean-square value as in (b) and obtained from the simulations.

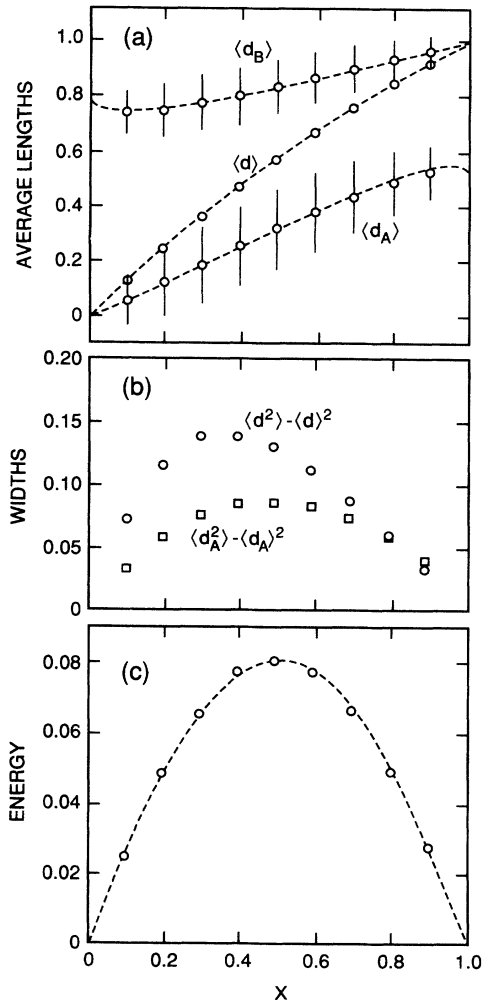

FIG. 8. Showing (a) average lengths $\langle d \rangle$, $\langle d_A \rangle$, and $\langle d_B \rangle$, (b) fluctuations in length, and (c) the energy in units of $K_A(L_B^0 - L_A^0)^2$ for a *correlated* triangular net with $K_B = 2K_A$. The dashed lines show results from effective-medium theory and the symbols represent simulation results. The length of the vertical lines in (a) represents the width of the A and B peaks, calculated as the root-mean-square value as in (b) and obtained from the simulations.

$$P(d)=\frac{1}{N}\sum_{ij=1}^{N}\delta(d-d_{ij}) \tag{53}$$

and

$$P(d_\alpha)=\frac{1}{N_\alpha}\sum_{ij=1}^{N_\alpha}\delta(d-d_{ij}),\quad \alpha=A,B\ . \tag{54}$$

We plot the distribution functions $P(d_A)$ and $P(d_B)$, obtained from the simulation data in Fig. 9. One sees that both $P(d_A)$ and $P(d_B)$ are *approximately* symmetric around the average values $\langle d_A\rangle$ and $\langle d_B\rangle$ in all cases. A closer examination shows that the distributions are *never* exactly symmetric except when the concentration $x=\frac{1}{2}$ and $K_A=K_B$. In Fig. 9(a), we have superimposed Gaussians with the exactly known weights, centers, and widths. Although the fits are good, especially in the wings, the deviations are significant. The moment ratio $\langle(\Delta d_\alpha)^4\rangle/\langle(\Delta d_\alpha)^2\rangle^2=2.97\pm0.01$, rather than the value of 3 that would be obtained for a Gaussian. It may be useful in practical applications, involving the analysis of experimental data, to use a Gaussian line shape.

We have examined the random case with $K_A=K_B$ more closely. A moment generating function can be written down in a way that closely parallels that used for a multilayer model of randomly intercalated compounds.[19] In fact, all the results there apply also to this case with suitable redefinitions. The final result is that

$$\begin{aligned}P(d_A)&=(1-x)Q(d_A-\langle d_A\rangle)\ ,\\ P(d_B)&=xQ(d_B-\langle d_B\rangle)\ ,\end{aligned} \tag{55}$$

so that the two distributions for the lengths of the A- and B-type bonds are identical, when shifted horizontally and rescaled vertically. The work in Ref. 19 also allows the moments to be written down

$$M_n=\langle(d_A-\langle d_A\rangle)^n\rangle=\langle(d_B-\langle d_B\rangle)^n\rangle\ , \tag{56}$$

and it is shown[19] that

$$\begin{aligned}M_2&=x(1-x)C_2\ ,\\ M_3&=x(1-x)(2x-1)C_3\ ,\\ M_4-3M_2^2&=x(1-x)[1-6x(1-x)]C_4\ .\end{aligned} \tag{57}$$

The only difference here from the work in Ref. 19 is in the constants C_n. We find that $C_2=\frac{2}{9}$ in agreement with Eq. (34), with $a^*(x)=\frac{2}{3}$. The quantities C_n for $n\geq3$ can be written down as multidimensional integrals in reciprocal space. We have not pursued this but rather focused our attention on the concentration dependence x in the moments (57). Note that the C_n are pure numbers. We have numerically obtained the moments and find that they are well fitted with the functional forms in (57) with $C_3=0.012\pm0.001$ and $C_4=0.0010\pm0.0006$. These numbers, especially C_4, are quite noisy and could be improved if more samples were averaged over. This intimate relation (55) between the A and B length distributions is not present in the other two cases examined in Fig. 9, and so it is killed when *either* $K_A\neq K_B$ *or* correlations are present, as shown in Figs. 9(b) and 9(c). A careful examination of these figures shows that the B distribution is wider in Fig. 9(b) and narrower in Fig. 9(c) than the A component. This is most easily established by computing the second moments.

The elastic moduli can also be computed for these networks by adding an appropriate incremental strain.[16] Care must be taken as the elastic moduli are proportional to the difference between two imprecisely known strain energies. Nevertheless, we were able to obtain good re-

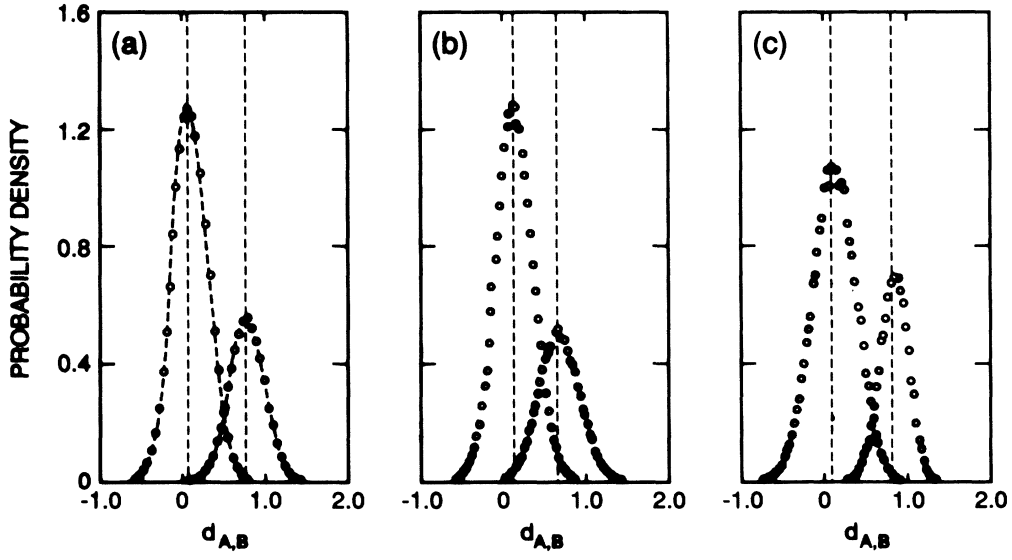

FIG. 9. Probability distributions of d_A and d_B for a triangular lattice from computer simulations. The vertical dashed lines show $\langle d_A\rangle$ and $\langle d_B\rangle$ with $\langle d_A\rangle<\langle d_B\rangle$. The panel (a) is for a *random* distribution of bonds and $K_A=K_B$. The dashed lines are Gaussian's having the correct weight, center, and width, which are known exactly and are given in the text. Panel (b) is for a *correlated* distribution of bonds with $K_A=K_B$, and (c) is for a *random* distribution of bonds and $K_B=2K_A$. In all cases, $x=0.3$ was the weight under the B peak and $1-x=0.7$ was the weight under the A peak.

sults as shown in Fig. 10 for the random case. The elastic moduli in two dimensions are directly proportional to the effective spring constant K. We take the elastic moduli to be proportional to K, as determined by Eq. (40). Of course when $K_A = K_B = K$, the elastic moduli are constant and come from the exact solution. In Fig. 10 the simulation results are compared with the exact results, shown as solid lines, and the effective-medium results shown as dashed lines. We have obtained simulation results for the correlated system that are fit equally as well as in Fig. 10, if the appropriate $a^*(x)$ is used in determining K using Eq. (40). The overall agreement is excellent in all cases, showing that the superposition principle for displacements is indeed valid for both the random and correlated cases. The elastic moduli do not depend upon the length mismatch and are the same as for a similar system with K_A and K_B, but with all bond lengths equal.

We have examined the effect of increasing the length difference $L_B^0 - L_A^0$. As long as the harmonic approximation is valid, we expect the results for the various lengths, *in the scaled variables d,* to be unchanged. We have tested this for the case when the spring constants are equal and find that the harmonic approximation is valid up to $(L_B^0 - L_A^0)/L_A^0 \approx 0.5$, when "pleating", as shown in Fig. 11, first occurs. This happens catastrophically and is defined by nearest-neighbor bonds crossing each other. This can occur in these models because there is no short-ranged repulsive force between sites. The transition to the pleated state can be thought of as a tunneling between two potential minima. As the length difference is increased, the pleated state is stabilized. Notice that these networks are constrained to remain in two dimensions. If motion were to be allowed in the third dimension, "crumpling,"[26] rather than pleating, would occur. The most remarkable result is that the harmonic approximation appears to be valid, to within 3%, for all quantities computed (energy, mean lengths, and fluctuations), right up to pleating, even though rather considerable length differences are involved.

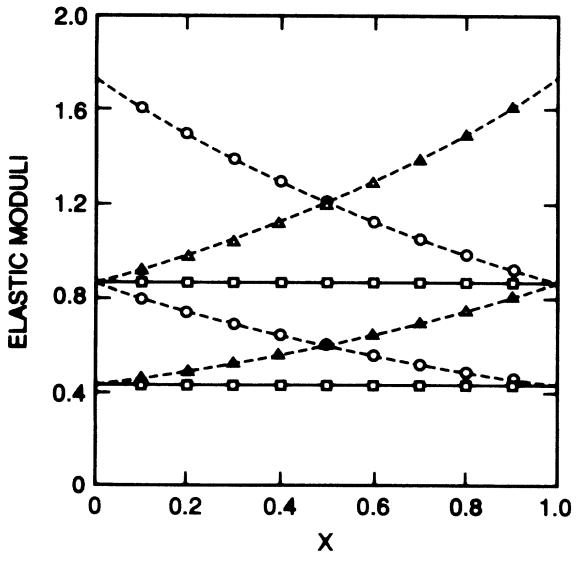

FIG. 10. Showing the bulk and shear moduli for randomly distributed bonds. The open symbols are from computer simulations, the solid lines are exact, and the dashed lines are from effective-medium theory. The squares are for $K_A = K_B = 1$, the circles are for $K_A = 2K_B = 2$, and the triangles are for $K_B = 2K_A = 2$. For each of the three cases, the shear modulus is less than the bulk modulus. For a perfect triangular net, the shear modulus is $\sqrt{3}K/4$ and the bulk modulus is $\sqrt{3}K/2$, with $K = K_A$ or K_B as appropriate.

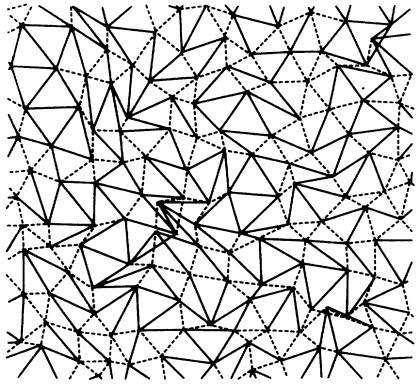

FIG. 11. Showing a piece of a pleated triangular network. The short bonds are shown as dashes and the long bonds by solid lines. The sample shown is the same as in Fig. 2 and has equal numbers of short and long bonds. However, the natural length of the long bonds is now double the natural length of the short bonds. The two spring constants K_A and K_B are equal.

Our conclusions are probably more general than just the present model and may be of use in gaining some quick insights into experiments. For example, Mikkelsen and Boyce[25] have made detailed high-quality measurements on semiconducting alloys like $Ga_{1-x}In_xAs$. From analyzing the x-ray diffraction results they find Vegard's law is closely obeyed for the mean bond length. From EXAFS experiments, they also find that the GaAs and AlAs mean bond lengths are linear in the composition x. Although the substitution of sites, rather than bonds, is more complex, we are tempted to interpret their experiments as evidence that the spring constants of GaAs and InAs are the same and that the solid solution is completely random. Of course the actual situation is more complex. It is not possible to describe GaAs and InAs with a single spring constant.

ACKNOWLEDGMENTS

We should like to thank Y. Cai, J. Chung, A. R. Day, and N. Rivier for interesting discussions. This work was supported in part by the National Science Foundation (NSF) under Grant No. DMR 87-14865.

APPENDIX A

In this appendix we describe how correlations are introduced between the bonds. Most of the ways of doing this lead to situations that do not permit an analytic determination of $a^*(x)$, for which *all* the pair-correlation functions must be known. The most obvious way to proceed would have been to use an Ising model.[22] How-

ever, the pair-correlation functions are only known locally and along certain principal directions for the triangular network.[22] Also a sum over all these pair-correlation functions would have had to be performed numerically out to all distances, in order to calculate $a^*(x)$. All statistical-mechanics models suffer from this same objection. In the work on correlated multilayers,[18] correlations were included in the direction perpendicular to the layers by using a one-dimensional Ising model for which all the two- and three-spin correlation functions are known. This form is sufficiently simple that the sums necessary for $a^*(x)$ can be done in closed form.

Faced with this situation, and wishing to investigate the effects of correlations, we modified an approach first suggested by Kirkpatrick,[27] and later used for an elastic network problem by Garboczi.[28] A random number r_i is associated with each site i, and $0<r_i<1$. The nearest-neighbor *bond* variables, $\sigma_{ij}=\pm 1$, are then chosen according to some algorithm involving only the two random variables r_i and r_j, associated with the sites at the ends of that bond. Here $\sigma_{ij}=-1$ signifies an A-type bond that occurs with probability $1-x$, and $\sigma_{ij}=-1$ signifies a B-type bond that occurs with probability x. This leads to positive correlations (clustering) between nearest-neighbor bonds, and no correlations between more distant bonds. This situation is somewhat counterintuitive but nevertheless correct.

In order to reproduce the single-defect behavior correctly, we use the following algorithm:

$$\text{if } r_i<p \text{ and } r_j<p \text{ then } \sigma_{ij}=1 ,$$
$$\text{if } r_i>p \text{ and } r_j>p \text{ then } \sigma_{ij}=-1 , \quad \text{(A1)}$$

otherwise $\sigma_{ij}=1$ with probability c .

Here c is a free parameter and p is directly related to the concentration x. By dividing up the (r_i,r_j) space into sectors, it is easy to show that

$$\langle \sigma_{ij} \rangle = 2x-1=(2p-1)+2p(1-p)(2c-1) . \quad \text{(A2)}$$

The pair correlations between nearest-neighbor bonds can be found by dividing the expanded space (r_i,r_j,r_k) into sectors. We find that

$$\langle \sigma_{ij}\sigma_{jk} \rangle - \langle \sigma_{ij} \rangle \langle \sigma_{jk} \rangle = p(1-p)[1-(2p-1)(2c-1)]^2 . \quad \text{(A3)}$$

In order that the pair correlations vanish more rapidly than x at small x, we choose $c=p$. The original algorithm of Kirkpatrick[27] does not have this desirable feature. Hence we have from (A2),

$$x=p^2(3-2p) , \quad \text{(A4)}$$

and p is seen to be a parameter that is determined by the concentration x. Note that (A4) can be rewritten

$$x(1-x)=[3+4p(1-p)][p(1-p)]^2 , \quad \text{(A5)}$$

which shows that $p(1-p)$ is a function of $x(1-x)$. The pair correlations (A3) become

$$\langle \sigma_{ij}\sigma_{jk} \rangle - \langle \sigma_{ij} \rangle \langle \sigma_{jk} \rangle = 16[p(1-p)]^3 \quad \text{(A6)}$$

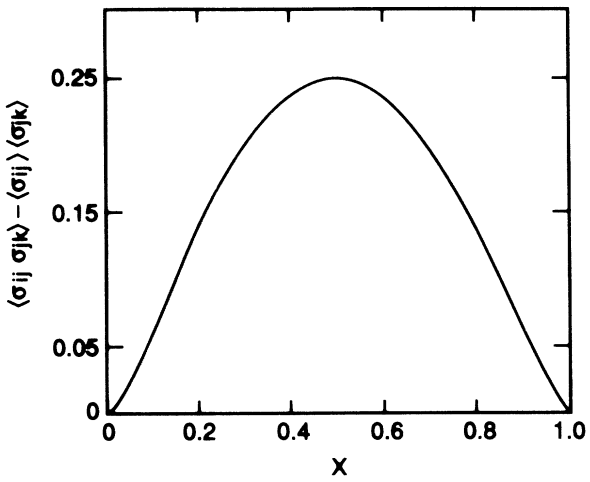

FIG. 12. Showing the correlation function $\langle \sigma_{ij}\sigma_{jk} \rangle - \langle \sigma_{ij} \rangle \langle \sigma_{jk} \rangle$ as a function of the concentration x for nearest-neighbor bonds, from the model described in Appendix A.

and are symmetric under the interchange $x \leftrightarrow 1-x$ as shown in Fig. 12. Note that the above formalism applies to any network in any dimension. In the triangular net, each bond is correlated with the 10 surrounding bonds that share a common vertex. For small x or $1-x$, (A6) becomes

$$\langle \sigma_{ij}\sigma_{jk} \rangle - \langle \sigma_{ij} \rangle \langle \sigma_{jk} \rangle = 2[4x(1-x)/3]^{3/2} . \quad \text{(A7)}$$

Although this correlation does vanish more rapidly than x to reproduce the single-defect limit, it unfortunately does not vanish as x^2 as the correct behavior in any reasonable structural model should. This is an inherent deficiency in the model that cannot be corrected by any simple modification of the algorithm (A1). Nevertheless, we have found the use of this model to be extremely instructive. At $x=\frac{1}{2}$, the pair correlations (A6) are maximum and given by

$$\langle \sigma_{ij}\sigma_{jk} \rangle - \langle \sigma_{ij} \rangle \langle \sigma_{jk} \rangle = \tfrac{1}{4} . \quad \text{(A8)}$$

This corresponds to an *attraction* between like bonds. In a bipartite lattice it would be possible to change the sign of these correlations by introducing a sign change on every other bond. This is not possible in the triangular net because of the presence of triangles.

APPENDIX B

We give details of the parameters used in the computer simulations. We have used the relaxation method.[17] All calculations were carried out on triangular networks with periodic boundary conditions and with $L_A^0=1.0$ and $L_B^0=1.01$, except in Sec. VI where the effect of larger length differences was investigated. For $K_A \neq K_B$, the networks were 30 by 34 bond lengths in size, while for $K_A=K_B$ we used larger 40 by 46 networks to better test the exact theory. Averages were taken over ten independent configurations, except for the length distribution data when $K_A=K_B$ at $x=0.3$ in Fig. 9 where 30 independent configurations were used. These same parameters were used for both the random and the correlated cases. Approximately 75 h of CYBER 205 time was consumed for this project.

*Permanent address: Physics and Astronomy Department and Center for Fundamental Materials Research, Michigan State University, East Lansing, MI 48824.

[1]H.-J. Herzog, L. Csepregi, and H. Seidel, J. Electrochem. Soc.: Solid State Sci. Technol. **131**, 2969 (1984).

[2]Hiroyuki Hirayama, Toru Tatsumi, and Naoaki Aizaki, Appl. Phys. Lett. **52**, 1335 (1988).

[3]M. Stutzmann, J. Harsanyi, A. Breitschwerdt, and C. P. Herrero, Appl. Phys. Lett. **52**, 1667 (1988).

[4]P. G. Klemens, F. W. Clinard, Jr., and R. J. Livak, J. Appl. Phys. **62**, 2062 (1987).

[5]D. J. Olego, H. Baumgart, and G. K. Celler, Appl. Phys. Lett. **52**, 483 (1988).

[6]A. Seidel, S. Massing, B. Strehlau, and G. Linker, Phys. Rev. B **38**, 2273 (1988).

[7]T. Egami and Y. Waseda, J. Non-Cryst. Solids **64**, 113 (1984).

[8]*Glass: Science and Technology,* edited by D. R. Uhlmann and N. J. Kreidl (Academic, New York, 1980), Vol. 5.

[9]K. A. Cerqua, S. D. Jacobs, and A. Lindquist, J. Non-Cryst. Solids **93**, 361 (1987).

[10]The compressive stress on the surface is, of course, balanced by tensile stress in the interior, so that the macroscopic stress is still zero.

[11]Brian R. Lawn and Edwin R. Fuller, Jr., J. Mater. Sci. **19**, 4061 (1984).

[12]David H. Roach and Alfred R. Cooper, J. Am. Ceram. Soc. **71**, C192 (1988).

[13]F. M. Lea, *The Chemistry of Cement and Concrete* (Chemical Publishing Co., New York, 1971).

[14]Jearl Walker, Sci. Am. **255** (4), 204 (1986).

[15]Kathleen A. Cerqua, Joseph E. Hayden, and William C. LaCourse, J. Non-Cryst. Solids **100**, 471 (1988).

[16]W. Tang and M. F. Thorpe, Phys. Rev. B **37**, 5539 (1988).

[17]S. Feng, M. F. Thorpe, and E. Garboczi, Phys. Rev. B **31**, 276 (1985).

[18]M. F. Thorpe, W. Jin, and S. D. Mahanti, Phys. Rev. B **40**, 10 294 (1989).

[19]Y. Cai, J. S. Chung, M. F. Thorpe, and S. D. Mahanti, Phys. Rev. B (to be published).

[20]R. P. Feynman, Phys. Rev. **56**, 340 (1939).

[21]L. Vegard, Z. Phys. **5**, 17 (1921).

[22]See, for example, L. Syozi, in *Phase Transitions and Critical Phenomena,* edited by C. Domb and M. S. Green (Academic, London, 1972), Vol. 1, p. 269.

[23]E. J. Garboczi and M. F. Thorpe, Phys. Rev. B **32**, 7276 (1985).

[24]M. F. Thorpe and E. J. Garboczi, Phys. Rev. B **35**, 8579 (1987).

[25]J. C. Mikkelsen, Jr. and J. B. Boyce, Phys. Rev. B **28**, 7130 (1983).

[26]M. Kardar and D. R. Nelson, Phys. Rev. Lett. **58**, 1289 (1987).

[27]S. Kirkpatrick, Rev. Mod. Phys. **45**, 574 (1973).

[28]E. J. Garboczi, Phys. Rev. B **36**, 2115 (1987).